PET Imaging of α4β2* Nicotinic Acetylcholine Receptors: Quantitative Analysis of ^{18}F-Nifene Kinetics in the Nonhuman Primate

Ansel T. Hillmer[1,2], Dustin W. Wooten[1,2], Maxim S. Slesarev[2], Elizabeth O. Ahlers[2], Todd E. Barnhart[1], Dhanabalan Murali[1,2], Mary L. Schneider[3], Jogeshwar Mukherjee[4], and Bradley T. Christian[1,2,5]

[1]Department of Medical Physics, University of Wisconsin-Madison, Madison, Wisconsin; [2]Waisman Brain Imaging Laboratory, University of Wisconsin-Madison, Madison, Wisconsin; [3]Department of Kinesiology, University of Wisconsin-Madison, Madison, Wisconsin; [4]Department of Radiological Sciences, University of California-Irvine, Irvine, California; and [5]Department of Psychiatry, University of Wisconsin-Madison, Madison, Wisconsin

The PET radioligand 2-fluoro-3-[2-((*S*)-3-pyrrolinyl)methoxy]pyridine (^{18}F-nifene) is an α4β2* nicotinic acetylcholine receptor (nAChR) agonist developed to provide accelerated in vivo equilibrium compared with existing α4β2* radioligands. The goal of this work was to analyze the in vivo kinetic properties of ^{18}F-nifene with both kinetic modeling and graphical analysis techniques. **Methods:** Dynamic PET experiments were performed on 4 rhesus monkeys (female; age range, 9–13 y) using a small-animal PET scanner. Studies began with a high-specific-activity ^{18}F-nifene injection, followed by a coinjection of ^{18}F-nifene and unlabeled nifene at 60 min. Sampling of arterial blood with metabolite analysis was performed throughout the experiment to provide a parent radioligand input function. In vivo kinetics were characterized with both a 1-tissue-compartment model (1TCM) and a 2-tissue-compartment model, Logan graphical methods (both with and without blood sampling), and the multilinear reference tissue model. Total distribution volumes and nondisplaceable binding potentials (BP_{ND}) were used to compare regional binding of ^{18}F-nifene. Regions examined include the anteroventral thalamus, lateral geniculate body, frontal cortex, subiculum, and cerebellum. **Results:** The rapid uptake and binding of ^{18}F-nifene in nAChR-rich regions of the brain was appropriately modeled using the 1TCM. No evidence for specific binding of ^{18}F-nifene in the cerebellum was detected on the basis of the coinjection studies, suggesting the suitability of the cerebellum as a reference region. Total distribution volumes in the cerebellum were 6.91 ± 0.61 mL/cm^3. BP_{ND} values calculated with the 1TCM were 1.60 ± 0.17, 1.35 ± 0.16, 0.26 ± 0.08, and 0.30 ± 0.07 in the anteroventral thalamus, lateral geniculate body, frontal cortex, and subiculum, respectively. For all brain regions, there was a less than 0.04 absolute difference in the average BP_{ND} values calculated with each of the 1TCM, multilinear reference tissue model, and Logan methods. **Conclusion:** The fast kinetic properties and specific regional binding of ^{18}F-nifene promote extension of the radioligand into preclinical animal models and human subjects.

Received Feb. 2, 2012; revision accepted Apr. 30, 2012.

For correspondence or reprints contact: Ansel T. Hillmer, Department of Medical Physics, University of Wisconsin-Madison, 1111 Highland Ave., Madison, WI 53705.

E-mail: ahillmer@wisc.edu

Published online Jul. 31, 2012.

Key Words: nAChR; PET; nicotine; ^{18}F-nifene; compartment modeling

J Nucl Med 2012; 53:1471–1480
DOI: 10.2967/jnumed.112.103846

Much work in the last 15 y has been devoted toward developing suitable PET radioligands to image α4β2* nicotinic acetylcholine receptors (nAChRs). These ligands bind with varying affinities to nAChRs containing either the β2 or α4 subunit, but most commonly to the α4β2 subtype, resulting in the notation α4β2*. The impetus for developing these probes stems from the interest in this receptor system's involvement in neurodevelopment, tobacco and alcohol addiction, and neuropathology. The disruption of cholinergic neurotransmission has been implicated in Alzheimer disease, leading to the application of acetylcholinesterase inhibitors as a treatment option for the symptoms of Alzheimer disease (*1,2*). Evidence of declining nAChR densities has been associated with Alzheimer disease, Parkinson disease, and healthy aging (*3,4*). Alterations from normal nAChR functioning have been implicated in other neurodegenerative diseases, including epilepsy (*5*), tobacco abuse (*6*), schizophrenia (*7*), and deficiencies in neurodevelopment, such as effects due to fetal alcohol exposure (*8*).

^{11}C-nicotine was the first radioligand developed for targeting α4β2* nAChR binding; however, it was found to have high nonspecific binding and rapid dissociation, rendering it unsuitable for PET studies (*9*). The radioligand 2-^{18}F-FA-85380 (2-^{18}F-FA) has been used the most extensively for PET studies of α4β2* nAChRs (*10,11*). Because of its slow in vivo behavior, PET experiments using 2-^{18}F-FA require more than 5 h of imaging for accurate measurement of α4β2* nAChR binding throughout all regions of the brain (*12*). Applications of this radioligand for PET studies have included studies of healthy aging (*13*), Alzheimer disease (*14*), Parkinson disease (*15*), and epilepsy (*16*).

The prolonged scanning procedures required for 2-^{18}F-FA quantification has spurred the development of various new α4β2* nAChR radioligands with faster kinetic properties, including both agonists and antagonists (*17*). Agonist radioligands, in particular, are of great interest because other receptor systems, including the dopamine and serotonin systems, have found agonist radioligands to exhibit increased sensitivity to competing endogenous neurotransmitter levels (*18,19*). This feature of nAChR radioligands will prove vital in evaluating acetylcholinesterase inhibitors for applications with Alzheimer disease. The α4β2* agonist radioligand 2-fluoro-3-[2-((*S*)-3-pyrrolinyl)methoxy]pyridine (^{18}F-nifene) was developed with the aim of improving on the success of 2-^{18}F-FA by creating an analog with faster kinetic properties and a similar binding profile (*20*). Previous studies have shown that ^{18}F-nifene exhibits fast transient equilibrium times of approximately 30 min, resulting in scanning procedures of less than an hour. Elevated ^{18}F-nifene binding in α4β2* nAChR-rich regions of the brain was also observed, with target-to-background binding levels suitable for applications in preclinical research (*21*). These studies preliminarily demonstrated the viability of ^{18}F-nifene PET experiments for translation into human subjects.

The goal of the present work was to extend previous studies with ^{18}F-nifene by examining its behavior in arterial blood to obtain quantitative measures of α4β2* nAChR binding with both model-based and graphical analysis techniques. The anteroventral thalamus and lateral geniculate body were analyzed because of their high binding levels and their role in a variety of neurodegenerative deficits, while the subiculum and frontal cortex were also examined as targets because of alterations in binding associated with Alzheimer disease and tobacco addiction (*2,22*). Blocking studies with unlabeled nifene were performed to evaluate the viability of the cerebellum to serve as a region of negligible detectable specific binding for techniques using reference region graphical analysis. These studies provide a necessary step toward validating the use of ^{18}F-nifene for studying the nAChR system during neurodevelopment and in disease-specific models.

MATERIALS AND METHODS

Radiochemistry

A secondary goal of this work was to improve the chemical purity of ^{18}F-nifene from previously reported methods (*20,21*). Specifically, high-performance liquid chromatography (HPLC) methods were modified to enhance the separation of the intermediate *N*-Boc-^{18}F-nifene from precursor after substitution. A 16-MeV PETtrace cyclotron (GE Healthcare) bombarded ^{18}O-enriched water with protons, creating ^{18}F-fluoride, which was separated from the enriched water with a QMA cartridge (Waters). After elution of ^{18}F with 1.2 mL of Kryptofix (Merck)–K_2CO_3 solution, the ^{18}F was azeotropically distilled in a customized chemistry processing control unit. Once dry, 0.5 mg of nitro precursor (2-nitro-3-[2-((*S*)-*N*-*tert*-butoxycarbonyl-3-pyrroline)methoxy]pyridine; ABX) in 250 μL of anhydrous acetonitrile and 150 μL of anhydrous dimethylsulfoxide was added for the reaction, which was heated to 120°C for 10 min. The mixture was then extracted with 4 mL of methylene chloride and passed through a neutral alumina Sep-Pak (Waters). The methylene chloride was dried and the product purified with HPLC. The use of a new separation method—consisting of a C-18 Prodigy column (10 μm, 250 × 10 mm; Phenomenex) with a mobile phase of 55% 0.05 M sodium acetate, 27% methanol, and 18% tetrahydrofuran at a flow rate of 8.0 mL/min—was incorporated into the ^{18}F-nifene purification. This HPLC method was previously developed for the synthesis of ^{18}F-MPPF, a serotonin 5-hydroxytryptamine subtype 1A radioligand whose precursor also contains a *nitro*-leaving group (*23*). Retention time of the *N*-Boc-^{18}F-nifene was approximately 14 min. The collected eluate (~5 mL) was then diluted in 50 mL of water, trapped on a C-18 Sep-Pak (Waters), and eluted with 1 mL of acetonitrile. Deprotection was performed with the addition of 200 μL of 6 N HCl, followed by heating at 80°C for 10 min. The mixture was then dried and pH adjusted to 7.0 with sodium bicarbonate. Ethanol (0.5 mL) and sterile saline were added for a total volume of 10 mL. This final product was purified with a preconditioned C-18 Sep-Pak (Waters) to remove any residual intermediate species (i.e., remaining *Boc*-protected product), followed by sterile filtration with a 0.22-μm Millipore filter for final formulation.

Subjects

PET scans with ^{18}F-nifene were acquired for 4 *Macaca mulatta* (rhesus monkey) subjects (4 females; weight range, 6.6–11.9 kg). All housing and experimental procedures obeyed institutional guidelines and were approved by the institutional animal care and use committee. Subjects were anesthetized before PET procedures with ketamine (10 mg/kg intramuscularly) and maintained on 1%–1.5% isoflurane for the duration of the experiment. Atropine sulfate (0.27 mg intramuscularly) was administered to minimize secretions. Body temperature, breathing rate, heart rate, and blood oxygen saturation levels were recorded for the duration of the experiment. The radiotracer was administered via bolus injection in the saphenous vein, and arterial blood samples were withdrawn from the tibial artery in the opposing limb. After completion of the experiment, the subject was returned to its cage and monitored until fully alert.

Data Acquisition

A Concorde microPET P4 scanner was used for the acquisition of PET data. This scanner has an axial field of view of 7.8 cm, a transaxial field of view of 19 cm, and a reported in-plane spatial resolution of 1.75 mm (*24*), which is slightly degraded to a 2.80-mm spatial resolution in the reconstructed image using the described experimental conditions and processing methods. The subject's head was held in a stereotactic headholder to obtain consistency in subject placement. A 518-s transmission scan was then acquired with a ^{57}Co rotating point source. Data acquisition began simultaneously with a bolus injection of 89–126 MBq (2.4–3.4 mCi) of ^{18}F-nifene and continued for 60 min. A second injection of 76–124 MBq (2.1–3.4 mCi) of ^{18}F-nifene mixed with unlabeled nifene was administered at 60 min to examine specific binding in the cerebellum. Details of each study are presented in Table 1.

For blood analysis, a 2″ NaI(Tl) well counter cross-calibrated with the PET scanner was used for radioactivity assay. Arterial blood was obtained in 500-μL volumes, with rapid sampling immediately after each ^{18}F-nifene injection and slowing to 10-min sampling by the end of the experiment. Once withdrawn, whole-

TABLE 1
Summary of Experiment Protocols

Subject no.	Subject mass (kg)	First injection		Second injection	
		Specific activity (GBq/μmol)	Injected dose (MBq)	Specific activity (GBq/μmol)	Injected dose (MBq)
M1	6.6	255	114	1. 7	113
M2	6.7	160	126	6.8	124
M3	11.9	>400	99	7.4	78
M4	8.6	120	89	0.56	76

Specific activities reported here are recorded at time of injection.

blood samples were mixed with 50 μL of heparinized saline, assayed for radioactivity, and centrifuged for 5 min. Plasma samples in 250-μL volumes were extracted, mixed with 50 μL of sodium bicarbonate, and assayed for radioactivity. To denature the proteins in the plasma, 1 mL of acetonitrile was added to the samples, followed by 30 s of centrifugation. The supernatant was extracted in volumes of 850 μL for radioactivity assay. Select samples were concentrated and spotted on aluminum-backed silica gel thin-layer chromatography (TLC) plates (Whatman). The plates were developed in a mobile phase of 50% methanol:50% 0.1 M ammonium acetate and exposed to a phosphor plate for at least 3 h. Plates were read with a Cyclone storage phosphor system (PerkinElmer) to determine the relative concentrations of metabolites in the plasma for each sample.

To account for radiometabolites, TLC data were analyzed with ImageJ software (National Institutes of Health), and the fraction of radioactivity in the ^{18}F-nifene peak relative to the total spotted radioactivity was measured for each sample. The measured time course of the parent ^{18}F-nifene in the plasma was parameterized by fitting the data to a biexponential function, producing a unique parent curve for each subject. This function describing the fraction of nonmetabolized parent was then applied as a correction to the radioactivity measured in the acetonitrile extract to produce values conveying the time course of ^{18}F-nifene parent present in the arterial blood. To examine the sensitivity of compartment-model parameter estimates to variations in the metabolite correction, analysis of the cerebellum region was also performed with a group-based (averaged) metabolite correction.

Plasma protein binding was examined with Centrifree ultrafiltration units (Millipore) to determine the free fraction of radioligand in the plasma. Before the administration of radiotracer, blood was drawn from subjects and centrifuged to yield a 250-μL plasma sample. ^{18}F-nifene was added to each sample in 25-μL volumes, and samples were incubated for 15 min at 37°C before separation, which occurred via ultrafiltration for 15 min at 2,000*g*. A similar procedure was performed with 250 μL of saline to correct for nonspecific binding of the radioligand to the filtration unit. The stability of the free fraction has not yet been fully characterized for ^{18}F-nifene and was therefore not incorporated into the subsequent analysis of the data; it is reported solely to provide additional information concerning the in vivo behavior of ^{18}F-nifene.

Data Analysis

PET data were binned from list mode into time frames of 8 × 30 s, 6 × 1 min, 24 × 2 min, 12 × 30 s, 6 × 1 min, and 18 × 2 min. The sinograms were reconstructed with 2-dimensional filtered backprojection using a 0.5-cm^{-1} ramp filter. Corrections for arc, scatter, attenuation, and scanner normalization were applied during reconstruction. The reconstructed images were processed with a denoising algorithm (*25*) using a 3 × 3 × 4 voxel filtering kernel. The final images had a matrix size of 128 × 128 × 63 corresponding to voxel dimensions of 1.90 × 1.90 × 1.21 mm.

Circular regions of interest were drawn over brain regions defined on the PET images. Cerebellum regions of interest were hand drawn on early summed images (0–8 min) with 4-voxel-diameter circles over 3 consecutive transverse slices to include mainly gray matter while avoiding the vermis region, resulting in a region volume of 663 mm^3 (152 voxels). Regions of high and moderate binding were identified in late summed images, from 20 to 40 min. Two general regions were selected from the thalamus, the anteroventral thalamus and lateral geniculate body, both drawn with 3-voxel-diameter circles over 3 consecutive transverse slices, yielding corresponding volumes of 231 mm^3 (53 voxels) for the anteroventral thalamus and 161 mm^3 (37 voxels) for the lateral geniculate body. The frontal cortex was identified with 4-voxel-diameter circles over 3 consecutive sagittal slices, resulting in a volume of 763 mm^3 (175 voxels), whereas the subiculum was delineated with 3-voxel-diameter circles over 3 consecutive transverse planes, giving a volume of 314 mm^3 (72 voxels). Time–activity curves were extracted for all regions of interest.

Model-based and graphical analysis methods were both applied for the analysis of the ^{18}F-nifene PET data. One-tissue- and 2-tissue-compartment models (1TCM and 2TCM, respectively) were used for the model-based analysis. The compartment-model analyses are described by the following equations:

$$\text{1TCM: } \frac{dC_T}{dt} = K_1 C_A - k_2' C_T$$

$$\text{2TCM: } \frac{dC_{ND}}{dt} = K_1 C_A - \left(k_2 + k_3\right) C_{ND} + k_4 C_S$$

$$\frac{dC_S}{dt} = k_3 C_{ND} - k_4 C_S,$$

where C_A is the concentration of parent radioligand in the arterial plasma. K_1 (mL/min/mL) and k_2 (min^{-1}) describe plasma–to–tissue transport and plasma–to–tissue clearance, respectively. C_{ND} represents the concentration of radiotracer present in the nondisplaceable compartment, which contains both free and nonspecifically bound

radioligand, and C_S represents the concentration of radiotracer in the specifically bound compartment. Transfer between these compartments conveying the reversible process of specific binding is described by the association rate k_3 and the dissociation rate k_4, both of which have units of min^{-1}. The 1TCM contains only the concentration of total radioactivity in the tissue, C_T, and includes only the parameters K_1 and k_2'. In regions of negligible specific binding, k_2' is equal to k_2, whereas in regions with rapidly equilibrating specific binding, k_2' is equivalent to $k_2(1 + k_3/k_4)^{-1}$. Volumes of distribution (V_T) were calculated for each region using data from the high-specific-activity injection ($t < 60$ min) with the equation $V_T = K_1/k_2'$ for the 1TCM and $V_T = K_1/k_2(1 + k_3/k_4)$ for the 2TCM (*26*). V_T was also calculated with the Logan graphical method with blood sampling using a linearization time of $t^* = 20$ min for all regions to provide for comparison with a graphical analysis technique (*27*).

For modeling calculations, the decay-corrected PET signal in a given region of tissue represents $PET = C_{ND} + C_S + f_V C_{WB}$, where f_V is the fractional blood volume, assumed to be 0.04, and C_{WB} is the concentration of radioactivity in the whole blood. Parameter estimations were performed with COMKAT software (*28*) with configurations for the 1TCM and 2TCM. Model comparison was evaluated with the corrected Akaike information criteria (*cAIC*):

$$cAIC = 2k + n\ln\left(\frac{RSS}{n}\right) + \frac{2k(k+1)}{n-k-1},$$

where k is the number of parameters in the model, n is the number of observations used for the fit, and *RSS* is the residual sum of squares for the fit (*29*).

Analysis of data from the cerebellum included PET data for the second low-specific-activity ^{18}F-nifene injection ($t > 60$ min). The plasma input function from 15 to 60 min was fit to a biexponential function and then extrapolated out past the time of the second injection. These extrapolated values were then subtracted from the observed data to strip away the first injection's residual radioactivity from the second injection. A similar method was used to correct the cerebellum time–activity curves by fitting the cerebellum data from 20 to 60 min to a biexponential function and then subtracting the extrapolated data from the second injection. Cerebellum V_T values were calculated for the second injection with the compartment modeling techniques described, with distinct parameters determined for each separate injection.

Receptor-specific binding of ^{18}F-nifene was characterized by estimation of the binding potential (BP_{ND}). BP_{ND} values were calculated with 2 graphical analysis techniques, the Logan graphical method (*30*) and the multilinear reference tissue model (MRTM) (*31*). The 3 methods previously discussed for V_T calculation (1TCM, 2TCM, and Logan with blood sampling) were also used to result in 5 different approaches to calculate BP_{ND}. For approaches with V_T estimation, the relation $BP_{ND} = V_T/V_{ND} - 1$ was used, where V_{ND} is the volume of distribution for nondisplaceable uptake and is equivalent to the estimation $BP_{ND} = DVR - 1$ used in the reference region approaches. The cerebellum was assumed to be a reference region devoid of specific binding where $V_T = V_{ND}$, consistent with findings presented herein and those reported previously (*21,32*). Differences in parameter estimates between analysis methods were investigated by plotting BP_{ND} values calculated from a given method against each of the other methods and fitting the data to a line. The slope was then subjected to a linear regression t test to determine the deviation of the slope from unity.

Because Logan reference region analysis is widely used for binding quantification, the proper linearization time of this approach was closely examined. Values reported herein used a linearization time of $t^* = 20$ min for all regions and omitted the mean efflux term $\overline{k_2}$. The necessary time for stability of BP_{ND} values calculated with this method was examined by varying the length of data analyzed from 30 to 60 min. Additionally, the inclusion of $\overline{k_2} = 0.20\ min^{-1}$ and a $t^* = 5$ min was also examined to increase the number of points on the Logan plot for improved quantification.

RESULTS

Radiochemistry

The new HPLC purification procedure improved separation of the remaining nifene precursor from the intermediate *N*-Boc-^{18}F-nifene after substitution, as demonstrated by Figure 1. This modified first purification also eliminated the need for a second HPLC separation after deprotection, because this step could instead be performed with a simple C-18 Sep-Pak extraction. As a result, the overall synthesis time was reduced from 2.5 to 1.5 h, with overall batch yields ranging from 500 to 1,500 MBq, corresponding to a 10%–20% decay-corrected radiochemical yield. Chemical purities were improved by 380% with the new HPLC purification method, primarily from the elimination of the *N*-Boc species, whereas end-of-synthesis specific activities were consistently in excess of 200 GBq/μmol.

^{18}F-Nifene in Blood

^{18}F-nifene is rapidly metabolized in the plasma, with all radiolabeled metabolite species being more polar than the parent compound (Fig. 2). The radioactivity in the plasma due to presumed metabolites was predominately shown by 2 overlapping peaks. Parent radioligand concentrations in plasma quickly fell to 40% after 15 min and 25% in 50 min

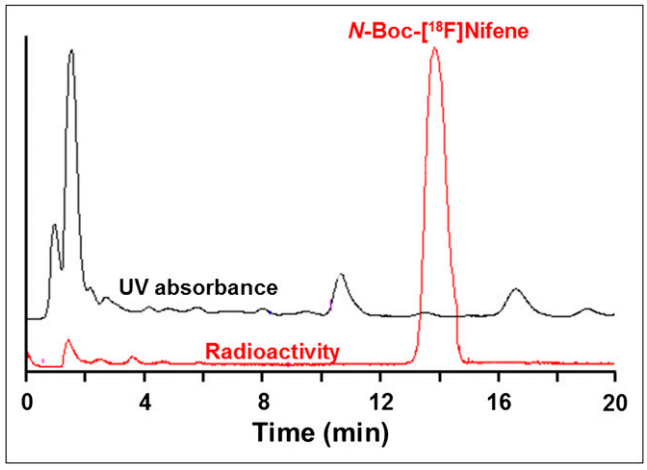

FIGURE 1. Semipreparative HPLC trace of *N*-Boc-^{18}F-nifene purification, performed with C-18 column and mobile phase of 55% 0.05 M NaAc, 27% MeOH, and 18% tetrahydrofuran at 8.0 mL/min. UV= ultraviolet.

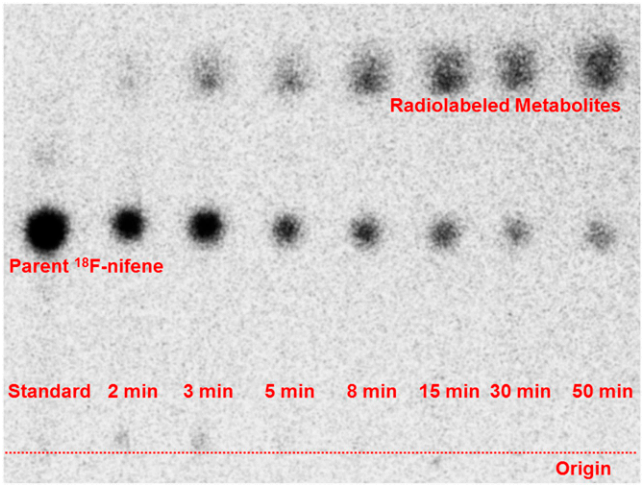

FIGURE 2. Typical radio-TLC profile of ^{18}F-nifene and its radiolabeled metabolites in plasma. Time after injection of each blood draw is noted for each sample. Experiments were performed on silica gel TLC plates with mobile phase of 50% methanol:50% 0.1 M ammonium acetate.

after ^{18}F-nifene administration (Fig. 3A). After the initial peak of ^{18}F-nifene, radioactive parent monotonically decreased, consistent with a 2-exponent function. The slower of these rates was 0.024 ± 0.003 min^{-1}, corresponding to a half-life in the plasma of 29 min (Fig. 3B). Plasma protein binding was also assessed to measure free fraction for nifene. An average of 46% ± 4% of the total radioactivity in the plasma was due to free ^{18}F-nifene.

V_T Estimations Using Arterial Input Function

The ^{18}F-nifene analysis with 1TCM and 2TCM using the measured arterial input parent functions revealed that the 2TCM was not statistically justified on the basis of *cAIC* in all regions, with the exception of 1 subject (M2). For this subject, however, V_T estimates were within 2% for both the 1TCM and the 2TCM methods. An illustrative example of a subject fit to the 1TCM is shown in Figure 4. V_T values were also estimated using the Logan graphical method with blood sampling and are shown with the 1TCM results in Table 2 (2TCM results are not shown because the 1TCM model was the preferred method). The thalamic regions of the anteroventral thalamus and lateral geniculate body yielded the highest ^{18}F-nifene V_T values of 17.95 ± 1.66 and 16.17 ± 1.64 mL/cm^3 with the 1TCM, whereas the frontal cortex and subiculum were found to have intermediate values of 8.69 ± 0.43 and 8.96 ± 0.48 mL/cm^3. The cerebellum had the lowest measure of V_T, 6.91 ± 0.61 mL/cm^3. The Logan method and 1TCM were in close agreement, with an average difference across all regions of 3.4% and a greatest discrepancy of 8%. The V_T values in the cerebellum calculated with a global metabolite-corrected input function differed from V_T calculated with individual corrections by less than 4% in all cases.

Cerebellum: Nifene Blocking Studies

Blocking studies with unlabeled nifene (i.e., low-specific-activity ^{18}F-nifene) were conducted to closely examine whether α4β2*-specific radioligand binding in the cerebellum could be detected. For 3 subjects, compartment modeling of the high-mass injection in the cerebellum yielded an average V_T of 6.8 ± 0.1 mL/cm^3—an average closely matching that of the high-specific-activity V_T for these subjects (6.7 ± 0.6 mL/cm^3). A visual comparison of the high- and low-specific-activity time courses in the cerebellum was also made by subtracting the residual signal of the first injection from the second and by normalizing the curves to the injected dose. An example is shown in Figure 5

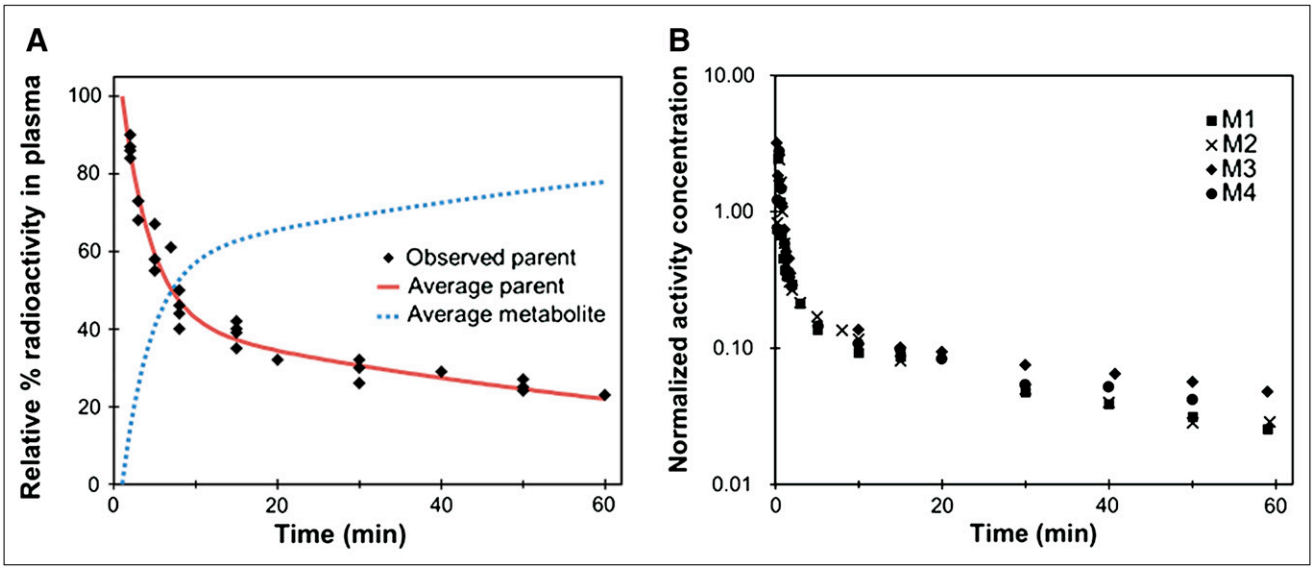

FIGURE 3. Time course of ^{18}F-nifene in blood. (A) Rate of metabolism of ^{18}F-nifene in plasma. Parent ^{18}F-nifene and radiolabeled metabolites are expressed as percentage of total radioactivity present in plasma. (B) Time–activity curve of ^{18}F-nifene parent in arterial plasma. Values are normalized by injected dose and multiplied by subject weight (kBq/mL/injected dose × kg).

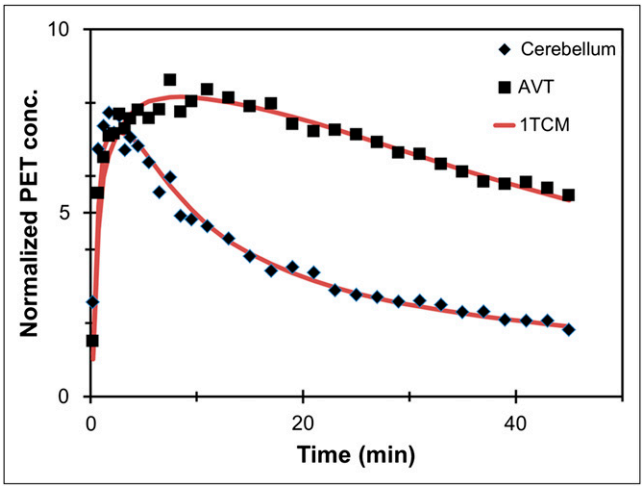

FIGURE 4. Sample time–activity curves (M4) of ^{18}F-nifene in rhesus monkey brain cerebellum and anteroventral thalamus, shown with fits generated by 1TCM. Values are normalized by injected dose and multiplied by subject weight (kBq/mL/injected dose × kg). AVT = anteroventral thalamus; conc = concentration.

for the subject for which blood sampling was unavailable for the second injection. All curves follow highly similar time courses, suggesting negligible perturbation due to the presence of blocking doses of nifene.

BP_{ND} Calculations

BP_{ND} values for the various methods are shown in Table 2. In the high-binding thalamic regions, values of 1.60 ± 0.17 and 1.35 ± 0.16 were measured with the 1TCM in the anteroventral thalamus and lateral geniculate body, respectively. The lower-binding regions of the subiculum and frontal cortex yielded respective values of 0.30 ± 0.07 and 0.26 ± 0.08. The largest difference in BP_{ND} between all methods for all regions was 15% (in the frontal cortex), whereas the average difference was 1%, suggesting good agreement between the various methods. No statistically significant ($\alpha < 0.1$) difference was detected between any of the methods presented here, indicating that all of the methods yielded consistent results.

Using a t* = 20 min with omission of $\overline{k_2}$ for the Logan reference region method, a scan time of at least 45 min yielded BP_{ND} values within 5% of those generated with a scan time of 60 min in all subjects under the aforementioned analysis conditions, indicating good stability of the metric. Additionally, the inclusion of $\overline{k_2}$ = 0.20 min^{-1} and a t* = 5 min for this analysis method revealed BP_{ND} values within 2% of values calculated without $\overline{k_2}$, indicating agreement between the 2 methods. A voxelwise image of BP_{ND} values calculated with the Logan graphical method was generated for visualization of ^{18}F-nifene uptake (Fig. 6).

TABLE 2
Measured V_T and BP_{ND} Values of ^{18}F-Nifene

		1TCM		Logan with blood sampling			
Subject no.	Region	V_T (mL/cm^3)	BP_{ND}*	V_T (mL/cm^3)	BP_{ND}	MRTM, BP_{ND}	Logan ref, BP_{ND}
M1	CB	7.44		7.68			
	AVT	20.41	1.74	20.83	1.71	1.70	1.68
	LG	18.56	1.50	19.11	1.49	1.45	1.44
	FC	9.04	0.22	9.31	0.21	0.20	0.20
	SB	9.26	0.25	9.50	0.24	0.24	0.24
M2	CB	6.28		6.13			
	AVT	16.98	1.70	16.43	1.68	1.67	1.67
	LG	15.29	1.44	15.11	1.46	1.45	1.44
	FC	8.06	0.28	7.92	0.29	0.28	0.28
	SB	8.25	0.31	8.03	0.31	0.30	0.30
M3	CB	6.48		6.18			
	AVT	16.93	1.61	15.54	1.51	1.54	1.52
	LG	14.97	1.31	13.97	1.26	1.26	1.27
	FC	8.89	0.37	8.27	0.34	0.34	0.34
	SB	9.10	0.40	8.56	0.39	0.38	0.38
M4	CB	7.42		7.49			
	AVT	17.47	1.35	17.86	1.38	1.44	1.35
	LG	15.85	1.14	16.29	1.17	1.20	1.14
	FC	8.78	0.18	9.11	0.22	0.21	0.20
	SB	9.25	0.25	9.33	0.25	0.25	0.24
Average ± SD	CB	6.91 ± 0.61		6.87 ± 0.83			
	AVT	17.95 ± 1.66	1.60 ± 0.17	17.67 ± 2.32	1.57 ± 0.15	1.59 ± 0.12	1.56 ± 0.15
	LG	16.17 ± 1.64	1.35 ± 0.16	16.12 ± 2.21	1.35 ± 0.15	1.34 ± 0.13	1.32 ± 0.15
	FC	8.69 ± 0.43	0.26 ± 0.08	8.65 ± 0.66	0.26 ± 0.06	0.26 ± 0.07	0.26 ± 0.07
	SB	8.96 ± 0.48	0.30 ± 0.07	8.86 ± 0.69	0.29 ± 0.07	0.29 ± 0.06	0.29 ± 0.07

*BP_{ND} for 1TCM was calculated as V_T/V_T(CB) − 1.
CB = cerebellum; AVT = anteroventral thalamus; LG = lateral geniculate body; FC = frontal cortex; SB = subiculum.

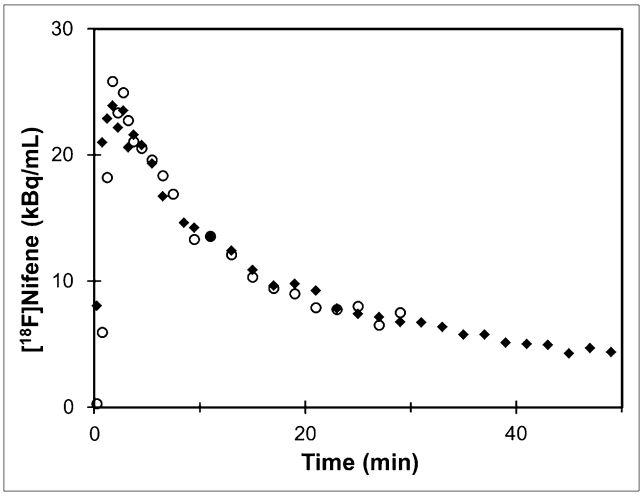

FIGURE 5. Representative time–activity curve of ^{18}F-nifene in cerebellum from high-specific-activity injection (♦) (specific activity, 210 GBq/μmol) and high-mass injection (○) (specific activity, 0.6 GBq/μmol) for 1 subject (M4). Values are normalized to injected dose.

DISCUSSION

^{18}F-nifene was developed to fulfill the need for a rapidly equilibrating α4β2* PET radioligand to advance research on this system by the neuroimaging community. The fast equilibration times of ^{18}F-nifene provide advantages in both greatly reducing the time of scan procedures and potentially detecting changes in endogenous acetylcholine levels. The 45-min imaging requirement for ^{18}F-nifene quantification is approximately 7-fold shorter than with the current α4β2* standard radiotracer, 2-^{18}F-FA, providing reductions in both experimental complexity and cost. More recently developed α4β2* radioligands, including ^{18}F-AZAN (*33*), ^{18}F-ZW-104 (*34*), and (−)-^{18}F-NCFHEB (*35*), show improvements over 2-^{18}F-FA both in increased binding levels and in reduced scan times, although each requires at least 90-min acquisitions for quantification, at least double the time required for ^{18}F-nifene. To build on our earlier studies, we have made significant improvements in radiochemical production and included the measurement of an arterial input function for use in the assay of specific binding and blocking studies with unlabeled nifene.

Arterial blood samples were acquired to examine the time course of ^{18}F-nifene available to the tissue and to quantify the presence of radiolabeled metabolites. Radio-TLC provided a well-separated profile of ^{18}F-nifene and radiolabeled metabolites, which allowed for characterization of radiolabeled species in the plasma while avoiding the use of HPLC analysis due to poor data quality resulting from low counting rates and injectate purification. Metabolism of ^{18}F-nifene occurred rapidly at first and then slowed to a metabolism rate with a half-life of 63 min. The increase of radiolabeled metabolites in arterial blood samples was consistent between all subjects, ranging between 68% and 74% at 30 min after injection. Differences in V_T in the cerebellum between the global and individual metabolite-corrected input functions were less than 4%, indicating that a moderate level of uncertainty could be tolerated in the measurement of radiolabeled metabolites. This finding suggests the potential use of a global parent metabolite correction, although additional validation would be required to examine age and sex-dependent variations in nifene metabolism. All detected radiolabeled metabolites were less lipophilic than the ^{18}F-nifene parent, suggesting that these metabolites cross the blood–brain barrier at a substantially lower rate than nifene. These observations are in agreement with previous studies of ^{18}F-nifene and its metabolites in the rat brain (*36*). Additionally, the ratio of radioactivity in the cerebellum to radioactivity of the parent ^{18}F-nifene in the plasma was found to be constant or slowly decreasing after 40 min, suggesting that there was no buildup of radiolabeled metabolites in the brain.

The possible presence of α4β2* binding in the cerebellum was examined by introducing a second administration of ^{18}F-nifene coinjected with unlabeled nifene. Previously, it was found that 0.03 mg (−)nicotine per kilogram qualitatively had no effect on cerebellum time–activity curves, suggesting the suitability of the cerebellum as a reference region (*21*). The work presented herein confirms this result using quantitative analysis performed with blood sampling. For the 3 subjects for which blood sampling was available to the end of the study, the introduction of high-mass nifene yielded V_T values (6.8 ± 0.1 mL/cm^3) that were consistent

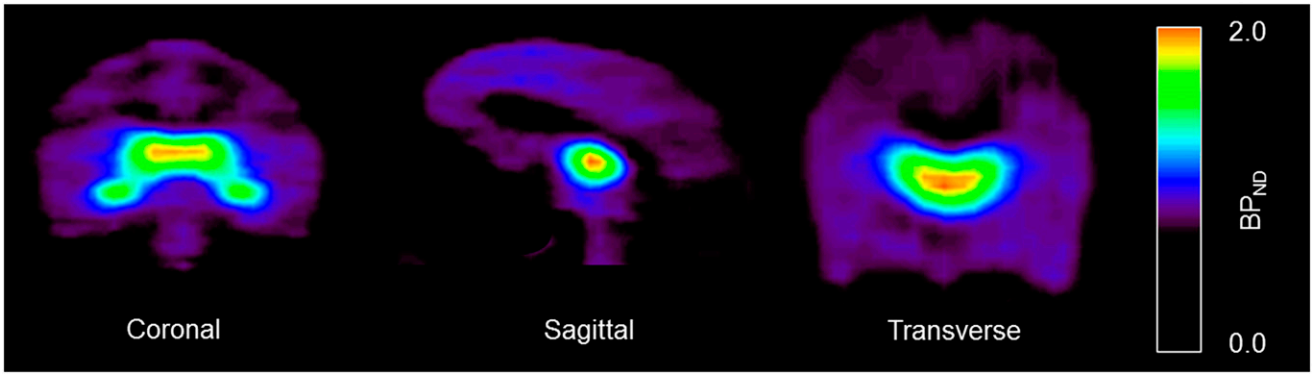

FIGURE 6. Specific binding of ^{18}F-nifene in rhesus monkey. Slices were chosen to focus on visualization of thalamus. Images were generated using voxelwise calculation of BP_{ND} with Logan graphical method.

with the values calculated from the first injection (6.7 ± 0.6 mL/cm^3) with the same 1TCM analysis, found here to be appropriate in evaluating regions of elevated ^{18}F-nifene binding. The similarity in V_T despite high levels of unlabeled nifene suggests that the specific binding component (V_S) in the cerebellum is lower than the sensitivity limits of the PET scanner and analysis techniques used here. This finding of a negligible V_S is in agreement with other studies examining 2-^{18}F-FA in the cerebellum of the rhesus monkey (*32*). Other PET studies have found small but significant cerebellar α4β2* nAChR expression in baboons (*10*) and humans (*12*), rendering the cerebellum problematic as a reference region in these species. The moderate BP_{ND} values of ^{18}F-nifene, however, may allow for the use of a valid reference region in humans in white matter regions such as the corpus callosum or the pons, as previously demonstrated with 2-^{18}F-FA (*14*). We briefly examined the corpus callosum as a reference region with the present data, however, the lack of MRI data resulted in high noise from the extracted time–activity curves and consequently higher variability in thalamic BP_{ND} values than that presented herein.

In brain regions with elevated ^{18}F-nifene binding, compartment modeling yielded a similar quality of fitting results (i.e., sum of squares) with both the 1TCM and the 2TCM, suggesting that the additional parameters of the 2TCM were not statistically warranted as specified by the *cAIC*. The selection of the 1TCM in regions of elevated binding suggests a lack of binding parameter identification due to fast equilibration between the nondisplaceable and specifically bound compartments. This result was also found in previous PET studies with ^{11}C-nicotine (*9*), however, no other α4β2* nAChR radioligands to our knowledge exhibit this behavior. The fast kinetics of ^{18}F-nifene are also reflected in the short 45-min scanning procedure requirement, which is advantageous in minimizing discomfort to the subjects when extending these imaging methods to diseased populations. The rapid binding and dissociation of ^{18}F-nifene may also provide increased sensitivity of ^{18}F-nifene binding to changes in endogenous levels of acetylcholine in vivo, as previously observed by in vitro work with acetylcholinesterase inhibitors (*37*).

BP_{ND} values were highest in thalamic regions of the brain, with intermediate levels of binding in the frontal cortex and subiculum. The level of ^{18}F-nifene binding in the frontal cortex was consistently lower than that of the subiculum. Similarly, the reduction in specific binding after the second (high-mass) ^{18}F-nifene injection followed the same rank order decrease across these regions. Furthermore, in the study with the lowest receptor occupancy by unlabeled ligand, the measured occupancy in the frontal cortex (24%) and subiculum (31%) compared well with the value measured in the thalamus (34%). Although the coefficient of variation across the 4 subjects was slightly higher in the intermediate-binding regions (~30%) than in the anteroventral thalamus (11%), the consistent rank order and agreement in receptor occupancy levels in the frontal cortex and subiculum suggest that ^{18}F-nifene provides adequate sensitivity to α4β2* binding in regions of intermediate uptake. We therefore do not rule out potential applications of ^{18}F-nifene in detecting small changes in α4β2* nAChR density in cortical regions, such as findings examining 2-^{18}F-FA uptake in patients with Alzheimer disease (*14*). Partial-volume effects should be considered in these cortical and hippocampal regions, particularly in patients with brain atrophy. The lack of MRI data prevented the application of a partial-volume correction in the present analysis, which could have resulted in underestimation of BP_{ND} values.

Comparison of V_{ND} between ^{18}F-nifene and other α4β2* radioligands provides insight into the differences in their imaging properties. Multiple-injection studies of 2-^{18}F-FA in baboons found V_{ND} values of 4.90 ± 0.46 g/mL in the thalamus and 4.25 ± 0.48 g/mL in the cerebellum (*38*). Studies of 2-^{18}F-FA in the rhesus monkey yielded a V_{ND} value of 4.32 ± 0.17 mL/cm^3 (when removing the correction for plasma free fraction) (*32*). Our present work indicates V_{ND} values of 6.9 ± 0.6 mL/cm^3 for ^{18}F-nifene in the rhesus monkey. Similarly, the clearance of radioligand from the blood is much faster for ^{18}F-nifene (0.024 ± 0.003 min^{-1}) than 2-^{18}F-FA (0.0056 ± 0.0017 min^{-1}). This large V_{ND} value for ^{18}F-nifene indicates that it is more readily taken up from the blood into the nondisplaceable compartment (e.g., free and nonspecifically bound radiotracer) and retained.

To gauge the level of α4β2* receptor occupancy in target regions, we have also examined data from the second injection in regions with specific binding. The rapid in vivo kinetics of ^{18}F-nifene allow for approximations of the change in specific binding after high-mass injections of nifene. These data can be used to estimate the in vivo equilibrium dissociation constant (K_{Dapp}) of ^{18}F-nifene for α4β2* nAChRs through the use of a Scatchard-type analysis (*39*). For this analysis, the 1TCM was used to calculate BP_{ND} values for both the first and the second injection in the thalamus. The ratio of these 2 values was used as a measure of in vivo receptor fractional occupancy (occupancy = $1 - BP_{ND(block)}/BP_{ND(baseline)}$). The free radioligand (F) was estimated by averaging the radioligand signal in the reference region at 20 min after coinjection (t = 80 min) to the end of the study and dividing by the specific activity. Plotting receptor occupancy against F yielded a nonlinear Scatchard plot, which was fit to the equation occupancy = $F/(K_{Dapp} + F)$ to estimate a value of K_{Dapp}, as shown in Figure 7. The analysis yielded a preliminary K_{Dapp} value of 3 ± 1 pmol/mL. This value is 2–3 times greater than the thalamic K_{Dapp} value for 2-^{18}F-FA reported by Gallezot et al. (*38*). When compared with 2-^{18}F-FA, the larger K_{Dapp} of nifene is consistent with its smaller BP_{ND}, assuming they compete for the same pool of receptors. Because of the small number of subjects and the uncertainty in the precise measurement of the free nifene concentration, this analysis provides only an approximation of K_{Dapp}; thus, additional studies will be required to establish the precision and variability

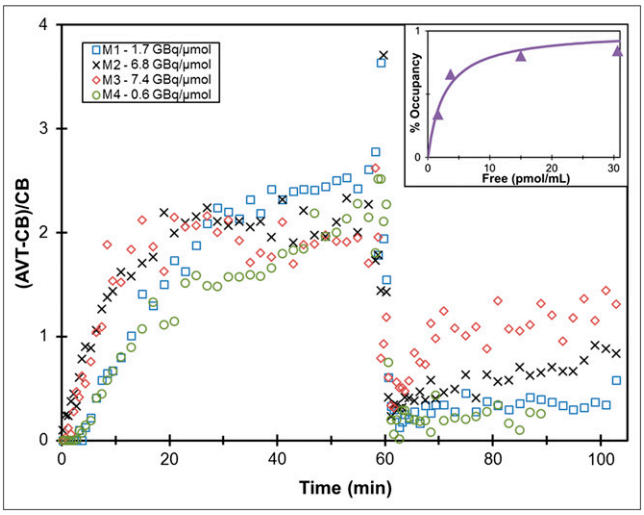

FIGURE 7. Change in thalamic binding with varying masses of unlabeled nifene. Thalamus-to-cerebellum ratio curves are shown, which include second high-mass ^{18}F-nifene injection at 60 min. Inset shows nonlinear Scatchard plot, illustrating calculation of approximate K_{Dapp} value. AVT = anteroventral thalamus; CB = cerebellum.

of this estimate. The present work provides a basis for guiding future experimental design of improved identification of receptor density (B_{max}) and K_{Dapp}.

CONCLUSION

The present work characterized the behavior of ^{18}F-nifene in the blood and found the 1TCM to most appropriately describe the data, further demonstrating the rapid equilibration times of ^{18}F-nifene and suggesting potential applications in measuring changes in endogenous acetylcholine levels. The cerebellum was quantitatively confirmed as a suitable reference region in the rhesus monkey, and sensitivity of ^{18}F-nifene to small changes in binding in areas of low uptake was found. These characteristics, combined with the requirement of 45-min scan times for accurate quantification, give ^{18}F-nifene unique advantages over other available α4β2* nAChR radioligands and promote the extension of ^{18}F-nifene to disease-specific animal models, with the potential for studies in human subjects.

DISCLOSURE STATEMENT

The costs of publication of this article were defrayed in part by the payment of page charges. Therefore, and solely to indicate this fact, this article is hereby marked "advertisement" in accordance with 18 USC section 1734.

ACKNOWLEDGMENTS

We thank the following for their contributions to this research: Professor R. Jerry Nickles and Drs. Jonathan Engle and Greg Severin for technical discussions and gracious assistance in isotope production and Julie Larson, Leslie Resch, and the staff at Harlow Center for Biological Psychology (RR000167) for assistance in animal handling and data acquisition. This work was supported by NIH grants AA017706 and CA142188. No other potential conflict of interest relevant to this article was reported.

REFERENCES

1. Gotti C, Clementi F. Neuronal nicotinic receptors: from structure to pathology. *Prog Neurobiol.* 2004;74:363–396.
2. Court J, Martin-Ruiz C, Piggott M, Spurden D, Griffiths M, Perry E. Nicotinic receptor abnormalities in Alzheimer's disease. *Biol Psychiatry.* 2001;49:175–184.
3. Burghaus L, Schütz U, Krempel U, Lindstrom J, Schröder H. Loss of nicotinic acetylcholine receptor subunits α4 and α7 in the cerebral cortex of Parkinson patients. *Parkinsonism Relat Disord.* 2003;9:243–246.
4. Hellström-Lindahl E, Court JA. Nicotinic acetylcholine receptors during prenatal development and brain pathology in human aging. *Behav Brain Res.* 2000;113:159–168.
5. Scheffer IE, Berkovic SF. The genetics of human epilepsy. *Trends Pharmacol Sci.* 2003;24:428–433.
6. Poirier M-F, Canceil O, Baylé F, et al. Prevalence of smoking in psychiatric patients. *Prog Neuropsychopharmacol Biol Psychiatry.* 2002;26:529–537.
7. Sacco KA, Bannon KL, George TP. Nicotinic receptor mechanisms and cognition in normal states and neuropsychiatric disorders. *J Psychopharmacol.* 2004;18:457–474.
8. Baer JS, Sampson PD, Barr HM, Connor PD, Streissguth AP. A 21-year longitudinal analysis of the effects of prenatal alcohol exposure on young adult drinking. *Arch Gen Psychiatry.* 2003;60:377–385.
9. Muzic RF, Berridge MS, Friedland RP, Zhu N, Nelson AD. PET quantification of specific binding of carbon-11-nicotine in human brain. *J Nucl Med.* 1998;39:2048–2054.
10. Valette H, Bottlaender M, Dollé F, et al. Imaging central nicotinic acetylcholine receptors in baboons with [^{18}F]fluoro-A-85380. *J Nucl Med.* 1999;40:1374–1380.
11. Gallezot J-D, Bottlaender M, Grégoire M-C, et al. In vivo imaging of human cerebral nicotinic acetylcholine receptors with 2-^{18}F-fluoro-A-85380 and PET. *J Nucl Med.* 2005;46:240–247.
12. Kimes AS, Chefer SI, Matochik JA, et al. Quantification of nicotinic acetylcholine receptors in the human brain with PET: bolus plus infusion administration of 2-[^{18}F]F-A85380. *Neuroimage.* 2008;39:717–727.
13. Ellis JR, Nathan PJ, Villemagne VL, et al. The relationship between nicotinic receptors and cognitive functioning in healthy aging: an in vivo positron emission tomography (PET) study with 2-[^{18}F]fluoro-A-85380. *Synapse.* 2009;63:752–763.
14. Kendziorra K, Wolf H, Meyer PM, et al. Decreased cerebral α4β2* nicotinic acetylcholine receptor availability in patients with mild cognitive impairment and Alzheimer's disease assessed with positron emission tomography. *Eur J Nucl Med Mol Imaging.* 2011;38:515–525.
15. Meyer PM, Strecker K, Kendziorra K, et al. Reduced α4β2*-nicotinic acetylcholine receptor binding and its relationship to mild cognitive and depressive symptoms in Parkinson disease. *Arch Gen Psychiatry.* 2009;66:866–877.
16. Picard F, Bruel D, Servent D, et al. Alteration of the in vivo nicotinic receptor density in ADNFLE patients: a PET study. *Brain.* 2006;129:2047–2060.
17. Horti AG, Gao Y, Kuwabara H, Dannals RF. Development of radioligands with optimized imaging properties for quantification of nicotinic acetylcholine receptors by positron emission tomography. *Life Sci.* 2010;86:575–584.
18. Narendran R, Hwang D-R, Slifstein M, et al. In vivo vulnerability to competition by endogenous dopamine: comparison of the D2 receptor agonist radiotracer (-)-N-[^{11}C]propyl-norapomorphine ([^{11}C]NPA) with the D2 receptor antagonist radiotracer [^{11}C]-raclopride. *Synapse.* 2004;52:188–208.
19. Paterson LM, Tyacke RJ, Nutt DJ, Knudsen GM. Measuring endogenous 5-HT release by emission tomography: promises and pitfalls. *J Cereb Blood Flow Metab.* 2010;30:1682–1706.
20. Pichika R, Easwaramoorthy B, Collins D, et al. Nicotinic α4β2 receptor imaging agents: part II. Synthesis and biological evaluation of 2-[^{18}F]fluoro-3-[2-((S)-3-pyrrolinyl)methoxy]pyridine (^{18}F-nifene) in rodents and imaging by PET in non-human primate. *Nucl Med Biol.* 2006;33:295–304.
21. Hillmer AT, Wooten DW, Moirano JM, et al. Specific α4β2 nicotinic acetylcholine receptor binding of [F-18]nifene in the rhesus monkey. *Synapse.* 2011;65:1309–1318.
22. Perry DC, Dávila-García MI, Stockmeier CA, Kellar KJ. Increased nicotinic receptors in brains from smokers: membrane binding and autoradiography studies. *J Pharmacol Exp Ther.* 1999;289:1545–1552.
23. Le Bars D, Lemaire C, Ginovart N, et al. High-yield radiosynthesis and preliminary in vivo evaluation of p-[^{18}F]MPPF, a fluoro analog of WAY-100635. *Nucl Med Biol.* 1998;25:343–350.
24. Tai C, Chatziioannou A, Siegel S, et al. Performance evaluation of the microPET P4: a PET system dedicated to animal imaging. *Phys Med Biol.* 2001;46:1845–1862.

25. Christian BT, Vandehey NT, Floberg JM, Mistretta CA. Dynamic PET denoising with HYPR processing. *J Nucl Med.* 2010;51:1147–1154.
26. Innis RB, Cunningham VJ, Delforge J, et al. Consensus nomenclature for in vivo imaging of reversibly binding radioligands. *J Cereb Blood Flow Metab.* 2007;27:1533–1539.
27. Logan J, Fowler JS, Volkow ND, et al. Graphical analysis of reversible radioligand binding from time-activity measurements applied to [*N*-^{11}C-methyl]-(-)-cocaine PET studies in human subjects. *J Cereb Blood Flow Metab.* 1990;10:740–747.
28. Muzic RF, Cornelius S. COMKAT: compartment model kinetic analysis tool. *J Nucl Med.* 2001;42:636–645.
29. Hurvich CM, Tsai C-L. Regression and time series model selection in small samples. *Biometrika.* 1989;76:297–307.
30. Logan J, Fowler JS, Volkow ND, et al. Distribution volume ratios without blood sampling from graphical analysis of PET data. *J Cereb Blood Flow Metab.* 1996;16:834–840.
31. Ichise M, Ballinger JR, Golan H, et al. Noninvasive quantification of dopamine D2 receptors with iodine-123-IBF SPECT. *J Nucl Med.* 1996;37:513–520.
32. Chefer SI, London ED, Koren AO, et al. Graphical analysis of 2-[^{18}F]FA binding to nicotinic acetylcholine receptors in rhesus monkey brain. *Synapse.* 2003;48:25–34.
33. Kuwabara H, Wong DF, Gao Y, et al. PET Imaging of nicotinic acetylcholine receptors in baboons with ^{18}F-AZAN, a radioligand with improved brain kinetics. *J Nucl Med.* 2012;53:121–129.
34. Valette H, Xiao Y, Peyronneau MA, et al. ^{18}F-ZW-104: a new radioligand for imaging neuronal nicotinic acetylcholine receptors—in vitro binding properties and PET studies in baboons. *J Nucl Med.* 2009;50:1349–1355.
35. Brust P, Patt JT, Deuther-Conrad W, et al. In vivo measurement of nicotinic acetylcholine receptors with [^{18}F]Norchloro-fluoro-homoepibatidine. *Synapse.* 2008;62:205–218.
36. Kant R, Constantinescu CC, Parekh P, et al. Evaluation of ^{18}F-nifene binding to α4β2 nicotinic receptors in the rat brain using microPET imaging. *EJNMMI Research.* 2011;1:6.
37. Easwaramoorthy B, Pichika R, Collins D, et al. Effect of acetylcholinesterase inhibitors on the binding of nicotinic α4β2 receptor PET radiotracer, ^{18}F-Nifene : a measure of acetylcholine competition. *Synapse.* 2007;61:29–36.
38. Gallezot J-D, Bottlaender MA, Delforge J, et al. Quantification of cerebral nicotinic acetylcholine receptors by PET using 2-[^{18}F]fluoro-A-85380 and the multi-injection approach. *J Cereb Blood Flow Metab.* 2008;28:172–189.
39. Farde L, Hall H, Ehrin E, Sedvall G. Quantitative analysis of D2 dopamine receptor binding in the living human brain by PET. *Science.* 1986;231:258–261.

JNM The Journal of NUCLEAR MEDICINE

PET Imaging of α4β2* Nicotinic Acetylcholine Receptors: Quantitative Analysis of ^{18}F-Nifene Kinetics in the Nonhuman Primate

Ansel T. Hillmer, Dustin W. Wooten, Maxim S. Slesarev, Elizabeth O. Ahlers, Todd E. Barnhart, Dhanabalan Murali, Mary L. Schneider, Jogeshwar Mukherjee and Bradley T. Christian

J Nucl Med. 2012;53:1471-1480.
Published online: July 31, 2012.
Doi: 10.2967/jnumed.112.103846

The Journal of Nuclear Medicine is published monthly.
SNMMI | Society of Nuclear Medicine and Molecular Imaging
1850 Samuel Morse Drive, Reston, VA 20190.
(Print ISSN: 0161-5505, Online ISSN: 2159-662X)

SNMMI SOCIETY OF NUCLEAR MEDICINE AND MOLECULAR IMAGING